Smooth terminating bands in ^{112}Te: Particle-hole induced collectivity

E. S. Paul,[1] K. Starosta,[2,*] A. O. Evans,[1] A. J. Boston,[1] H. J. Chantler,[1] C. J. Chiara,[2,†] M. Devlin,[3,‡] A. M. Fletcher,[4] D. B. Fossan,[2] D. R. LaFosse,[3] G. J. Lane,[2,§] I. Y. Lee,[5] A. O. Macchiavelli,[5] P. J. Nolan,[1] D. G. Sarantites,[3] J. M. Sears,[2] A. T. Semple,[1] J. F. Smith,[2,4,‖] C. Vaman,[2,¶] A. V. Afanasjev,[6,7,8] and I. Ragnarsson[7]

[1]*Oliver Lodge Laboratory, University of Liverpool, Liverpool L69 7ZE, United Kingdom*

[2]*Department of Physics and Astronomy, State University of New York at Stony Brook, Stony Brook, New York 11794-3800, USA*

[3]*Department of Chemistry, Washington University, St. Louis, Missouri 63130, USA*

[4]*Schuster Laboratory, The University of Manchester, Brunswick Street, Manchester M13 9PL, United Kingdom*

[5]*Nuclear Science Division, Lawrence Berkeley National Laboratory, Berkeley, California 94720, USA*

[6]*Department of Physics and Astronomy, Mississippi State University, Mississippi 39762, USA*

[7]*Department of Mathematical Physics, Lund Institute of Technology, P.O. Box 118, S-22100 Lund, Sweden*

[8]*Laboratory of Radiation Physics, Institute of Solid State Physics, University of Latvia, LV 2169 Salaspils, Miera str. 31, Latvia*

(Received 15 August 2006; published 10 January 2007)

The Gammasphere spectrometer, in conjunction with the Microball charged-particle array, was used to investigate high-spin states in ^{112}Te via ^{58}Ni(^{58}Ni, $4p\gamma$) reactions at 240 and 250 MeV. Several smooth terminating bands were established, and lifetime measurements were performed for the strongest one using the Doppler-shift attenuation method. Results obtained in the spin range 18–32$\hbar$ yield a transition quadrupole moment of $4.0 \pm 0.5 eb$, which corresponds to a quadrupole deformation $\varepsilon_2 = 0.26 \pm 0.03$; this value is significantly larger than the ground-state deformation of tellurium isotopes. It was also possible to extract a transition quadrupole moment for the yrast band in ^{114}Xe, produced via the ^{58}Ni(^{58}Ni, $2p\gamma$) reaction. A value of $3.0 \pm 0.5\, eb$ was found in the spin range 16–24$\hbar$, which corresponds to a quadrupole deformation $\varepsilon_2 = 0.19 \pm 0.03$. Cranked Nilsson-Strutinsky calculations are used to interpret the results.

DOI: 10.1103/PhysRevC.75.014308 PACS number(s): 21.10.Re, 23.20.Lv, 27.60.+j

I. INTRODUCTION

Deformed bands in $_{49}$In, $_{50}$Sn, $_{51}$Sb, $_{52}$Te, $_{53}$I, and $_{54}$Xe isotopes have been observed to high rotational frequency with decreasing moments of inertia. This structure feature, so-called smooth band termination [1], has been successfully interpreted using configuration-dependent cranking calculations [2], and confirmed through the measurement of quadrupole moments in such bands of ^{108}Sn and ^{109}Sb [3]. Proton particle-hole (p-h) excitations across the $Z = 50$ shell gap are able to induce quadrupole deformation in these nuclei at low spin, but the finite number of valence nucleons leads to termination of rotational bands into noncollective oblate states at spin $\sim 50\hbar$. Several new terminating bands have been established in ^{112}Te, extending the level scheme to a spin of 46$\hbar$ at an excitation energy approaching 29 MeV. Mean-level lifetime measurements have been performed for the strongest such band in ^{112}Te in the spin range 18–32$\hbar$ and clearly show evidence for large quadrupole deformation. This is in contrast to the ground-state band of ^{112}Te, which, similarly to other even-even tellurium isotopes, exhibits vibrational character typical of a weakly deformed shape.

II. EXPERIMENTAL DETAILS

Two experiments were carried out at the 88-Inch Cyclotron of the Lawrence Berkeley National Laboratory. In the first, thin-target experiment, high-spin states in $A \sim 110$ nuclei were populated with the ^{58}Ni(^{58}Ni, $x\alpha\, yp\, zn\, \gamma$) fusion-evaporation reaction at 250 MeV; 1.4×10^9 events were collected. The Gammasphere [4] γ-ray spectrometer, containing 83 HPGe detectors, was used in conjunction with the Microball [5] charged-particle detector and an array of 15 neutron detectors to provide clean exit channel selection by determining the number of evaporated particles (x, y, z). Gamma rays selected for ^{112}Te$(x = 0, y = 4, z = 0)$ were sorted into a Radware-format [6,7] cube (γ^3) for subsequent level-scheme construction.

By measuring the energies and directions of the four emitted protons using the Microball, it was possible to perform a thorough kinematic Doppler reconstruction [8] of the nuclear recoil vector; this approach yielded an improvement of typically 30% in the resolution of γ-ray transitions in ^{112}Te, as compared to the assumption that the recoils all traveled exactly in the direction of the beam axis. Indeed at a γ-ray energy of 1 MeV, the full-width half-maximum (FWHM) of a transition was reduced from $\sim$8.0 to $\sim$5.0 keV.

*Present address: National Superconducting Cyclotron Laboratory, Michigan State University, East Lansing, Michigan 48824.

†Present address: Department of Chemistry, Washington University, St. Louis, Missouri 63130.

‡Present address: Los Alamos National Laboratory, Los Alamos, New Mexico 87545.

§Present address: Department of Nuclear Physics, Research School of Physical Sciences and Engineering, Australian National University, Canberra ACT 0200, Australia.

‖Present address: School of Engineering and Science, University of Paisley, Paisley, PA1 2BE, United Kingdom.

¶Present address: National Superconducting Cyclotron Laboratory, Michigan State University, East Lansing, Michigan 48824.

In the second experiment, a target consisting of 1 mg/cm^2 of ^{58}Ni on a ^{208}Pb backing of thickness 15 mg/cm^2, was bombarded by a 240-MeV ^{58}Ni beam. Gammasphere containing 98 HPGe detectors was used in conjunction with the Microball charged-particle detector. The backed target was used to facilitate the measurement of mean-level lifetimes using the Doppler-shift attenuation method (DSAM) [9]. Escape-suppressed γ-ray events were recorded to magnetic tape, when an event contained a minimum of three γ rays was detected in prompt coincidence with a charged particle in the Microball. The initial 6.4×10^8 events were reduced to 2.4×10^8 events following the selection of the four proton exit channel through gating with the Microball.

III. RESULTS

A. Thin-target data

The level scheme deduced for ^{112}Te is shown in Fig. 1, with positive-parity structures shown mainly to the left and negative-parity structures shown to the right. The majority of the transitions in the structures labeled A–E had already been established in Ref. [10], but have now been extended to spin $\sim 30\hbar$. Spin and parity assignments are adopted from Ref. [10]. Five high-spin band structures, labeled 1–5 are also shown in Fig. 1. Relative to the 689 keV $2^+ \rightarrow 0^+$ transition, these five structures are measured to carry intensities of approximately 7.0, 1.0, 0.2, 1.0, and 0.5%, respectively. The lower portion of Band 1 was originally established in Ref. [10] and feeds into the ground-state Band A at the 8^+ and 10^+ levels. A two-step link is also observed into the 16^+ state of Band A via 925- and 415-keV transitions. A spectrum of Band 1 is shown in Fig. 2.

It has now been extended to $I^\pi = 46^+$, comprising 18 transitions, with some transitions around spin 30^+ reordered with respect to Ref. [10]. It can be seen that, around this spin, Band 1 is linked via several transitions to a strongly coupled structure, labeled Band 2, which has recently been presented in Ref. [11]. This latter band also feeds into Band A at the 18^+ and 20^+ levels. Spectra for Band 2 are shown in Fig. 3. Newly identified Bands 3, 4, and 5 represent three further sequences of transitions extending to high spin; spectra are shown in Fig. 4. It was not possible to uniquely link these bands into the ^{112}Te level scheme. Band 3 appears to decay into positive-parity states of Band A around spin $18\hbar$. Band 4 feeds negative-parity Band C at the 27^- level, in addition to the negative-parity Bands D and E at lower spins. Two transitions, of energies 1353 and 1351 keV appear to depopulate Band 4 at the (33^-) and (27^-) levels, respectively, although the exact decay paths into the known level scheme could not be unambiguously determined. The 1353-keV transition does, however, feed the high-energy 1439- and 1979-keV transitions that themselves feed Band C at 27^-. Band 5 feeds only the low-spin negative-parity Bands D and E. The absolute spins and parities of Bands 3, 4, and 5, shown in Fig. 1, are tentative and have been chosen following comparison to theoretical calculations, discussed in detail in Sec. IV below. The transition energies and adopted spin assignments for Bands 1–5 are summarized in Tables I and II.

B. Backed-target data

A γ ray that is emitted while the recoiling nucleus is slowing down in the target and backing material will exhibit a Doppler-shifted, and broadened, line shape. The magnitude of the shift

TABLE I. Measured energies and spin-parity assignments of γ-ray transitions assigned to the decoupled ($\Delta I = 2$) smooth terminating bands in ^{112}Te, as shown in Fig. 1. The relative channel intensity of each band is indicated as a percentage. Errors on the energies are estimated to be ± 0.3 keV, except those values quoted as integers which have errors ± 1 keV.

Band 1 (7.0%)		Band 3 (0.2%)		Band 4 (1.0%)		Band 5 (0.5%)	
E_γ (keV)	$I_i^\pi \rightarrow I_f^\pi$	E_γ (keV)	$I_i^\pi \rightarrow I_f^\pi$	E_γ (keV)	$I_i^\pi \rightarrow I_f^\pi$	E_γ (keV)	$I_i^\pi \rightarrow I_f^\pi$
751.6	$12^+ \rightarrow 10^+$	966	$(23^+ \rightarrow 21^+)$	860	$(23^- \rightarrow 21^-)$	867	$(20^- \rightarrow 18^-)$
758.6	$14^+ \rightarrow 12^+$	1019	$(25^+ \rightarrow 23^+)$	933.5	$(25^- \rightarrow 23^-)$	940	$(22^- \rightarrow 20^-)$
801.3	$16^+ \rightarrow 14^+$	1114	$(27^+ \rightarrow 25^+)$	1008.7	$(27^- \rightarrow 25^-)$	1021	$(24^- \rightarrow 22^-)$
862.4	$18^+ \rightarrow 16^+$	1218.9	$(29^+ \rightarrow 27^+)$	1124.0	$(29^- \rightarrow 27^-)$	1102	$(26^- \rightarrow 24^-)$
928.7	$20^+ \rightarrow 18^+$	1331.1	$(31^+ \rightarrow 29^+)$	1212.1	$(31^- \rightarrow 29^-)$	1206.3	$(28^- \rightarrow 26^-)$
998.2	$22^+ \rightarrow 20^+$	1470.4	$(33^+ \rightarrow 31^+)$	1310.7	$(33^- \rightarrow 31^-)$	1291.2	$(30^- \rightarrow 28^-)$
1071.8	$24^+ \rightarrow 22^+$	1612.6	$(35^+ \rightarrow 33^+)$	1394.0	$(35^- \rightarrow 33^-)$	1358.3	$(32^- \rightarrow 30^-)$
1146.4	$26^+ \rightarrow 24^+$	1777.6	$(37^+ \rightarrow 35^+)$	1518.5	$(37^- \rightarrow 35^-)$	1401.8	$(34^- \rightarrow 32^-)$
1217.7	$28^+ \rightarrow 26^+$	1920.8	$(39^+ \rightarrow 37^+)$	1676.1	$(39^- \rightarrow 37^-)$	1500.8	$(36^- \rightarrow 34^-)$
1291.2	$30^+ \rightarrow 28^+$	2071.0	$(41^+ \rightarrow 39^+)$	1875.8	$(41^- \rightarrow 39^-)$	1640.2	$(38^- \rightarrow 36^-)$
1363.8	$32^+ \rightarrow 30^+$			2105.5	$(43^- \rightarrow 41^-)$	1809.7	$(40^- \rightarrow 38^-)$
1500.8	$34^+ \rightarrow 32^+$			2327	$(45^- \rightarrow 43^-)$	1994.8	$(42^- \rightarrow 40^-)$
1624.8	$36^+ \rightarrow 34^+$					2185	$(44^- \rightarrow 42^-)$
1721.0	$38^+ \rightarrow 36^+$						
1806.7	$40^+ \rightarrow 38^+$						
1942.5	$42^+ \rightarrow 40^+$						
2105	$44^+ \rightarrow 42^+$						
2293	$46^+ \rightarrow 44^+$						

TABLE II. Measured energies and spin-parity assignments of γ-ray transitions assigned to the strongly coupled smooth terminating band in ^{112}Te, as shown in Fig. 1. The $\Delta I = 2$ signature components ($\alpha = 0, 1$) are listed together with the interlinking $\Delta I = 1$ dipole transitions. The relative channel intensity of the band is indicated by the percentage. Errors on the energies are estimated to be ± 0.3 keV, except those values quoted as integers which have errors ± 1 keV.

Band 2 (1.0%)							
$\alpha = 0$		$\alpha = 1$		Dipoles			
E_γ (keV)	$I_i^\pi \to I_f^\pi$	E_γ (keV)	$I_i^\pi \to I_f^\pi$	E_γ (keV)	$I_i^\pi \to I_f^\pi$	E_γ (keV)	$I_i^\pi \to I_f^\pi$
870.8	$22^+ \to 20^+$	941.5	$23^+ \to 21^+$	406	$21^+ \to 20^+$	465.1	$22^+ \to 21^+$
972.1	$24^+ \to 22^+$	1004.4	$25^+ \to 23^+$	476.4	$23^+ \to 22^+$	495.9	$24^+ \to 23^+$
1038.1	$26^+ \to 24^+$	1079.2	$27^+ \to 25^+$	507.9	$25^+ \to 24^+$	530.4	$26^+ \to 25^+$
1112.0	$28^+ \to 26^+$	1149.1	$29^+ \to 27^+$	548.8	$27^+ \to 26^+$	563.1	$28^+ \to 27^+$
1184.3	$30^+ \to 28^+$	1242.1	$31^+ \to 29^+$	586.0	$29^+ \to 28^+$	597.8	$30^+ \to 29^+$
1298.9	$32^+ \to 30^+$	1365.2	$33^+ \to 31^+$	644.3	$31^+ \to 30^+$	655.2	$32^+ \to 31^+$
1434.2	$34^+ \to 32^+$	1512.4	$35^+ \to 33^+$	710.1	$33^+ \to 32^+$	724.2	$34^+ \to 33^+$
1588.7	$36^+ \to 34^+$	1729.4	$37^+ \to 35^+$	788	$35^+ \to 34^+$	801	$36^+ \to 35^+$
1855	$38^+ \to 36^+$	2008	$39^+ \to 37^+$	928	$37^+ \to 36^+$		
2114	$40^+ \to 38^+$						

is related to the mean lifetime of the depopulated and feeding levels, together with the stopping powers of the slowing down medium. A measurement of the centroid shift of γ rays can thus be used to extract mean lifetimes of the levels by modeling the slowing-down process.

To first order, the Doppler-shifted energy E_s of a transition E_0 measured at an angle θ relative to the direction of the recoiling nucleus is,

$$E_s = E_0\left[1 + F(\tau)\frac{v_0}{c}\cos\theta\right], \tag{1}$$

where v_0 is the initial recoil velocity. The quantity $F(\tau)$ is an attenuation factor equal to $\bar{v}/v_0$, where $\bar{v}$ is the average recoil velocity when the γ ray is actually emitted. The initial recoil velocity v_0 was calculated using reaction kinematics; a value of $v_0 = 0.047c$ was obtained, assuming that the compound nucleus was formed in the center of the target. The mean lifetime τ of a nuclear level was obtained by comparing the measured value of $F(\tau)$, for a γ ray depopulating that level, with theoretical values calculated assuming a constant values of the in-band transition quadrupole moment Q_t. These calculations used the codes reported in Ref. [12] and used Ziegler stopping powers [13] to evaluate the slowing-down process of the recoiling nuclei in the target and backing material. It should be noted that these stopping powers may have systematic errors as large as 10–15%.

Events corresponding to the evaporation of four protons (^{112}Te) were selected by the Microball. Three gated asymmetric matrices were then created, with a gate set on the 1098 keV ($10^+ \to 8^+$) fully stopped γ ray, which links Band 1 to the ground-state Band A of ^{112}Te (see Fig. 1). The axes of the matrices contained (i) detectors located at a "forward" angle of the Gammasphere spectrometer, $\theta = 50.1^\circ$, sorted against all angles, (ii) detectors located at the complementary "backward" angle, $\theta = 129.9^\circ$, sorted against all angles, and (iii) detectors located at $\theta = 90^\circ$ sorted against all angles. Gates were placed on the 1098-, 752-, 759-, and 801-keV γ rays on the axis of each matrix containing all angles, and the resulting coincident γ-ray spectra at forward, backward, and 90° angles projected out, as shown in Fig. 5. From the forward and backward spectra, the centroids of Doppler-shifted γ-ray peaks could be extracted to calculate experimental fractional Doppler shifts $F(\tau)$.

Experimental $F(\tau)$ values are plotted in Fig. 6. Theoretical $F(\tau)$ curves are also drawn corresponding to constant transition quadrupole moments of 3.5, 4.0, and 4.5 eb, respectively. A value of $Q_t = 4.0 \pm 0.5\,eb$ best describes the experimental data and the corresponding mean-level lifetimes, calculated from

$$\tau(\text{ps}) = \frac{0.820}{|\langle I\,0\,2\,0|I-2\,0\rangle|^2 E_\gamma^5(\text{MeV})Q_t^2(eb)}, \tag{2}$$

are listed in Table III.

The value $Q_t = 4.0 \pm 0.5\,eb$ yields a quadrupole deformation of $\varepsilon_2 = 0.26 \pm 0.03$, assuming zero hexadecapole deformation ($\varepsilon_4 = 0$) and axial, prolate nuclear shape ($\gamma = 0^\circ$). The expressions relating Q_t to the deformation parameters

TABLE III. Level lifetimes extracted for Band 1 of ^{112}Te, assuming a contant $Q_t = 4.0 \pm 0.5\,eb$.

Spin I	$E_\gamma\,[I \to I-2]$ (keV)	τ (ps)
18	862	0.304^{+94}_{-64}
20	929	0.207^{+64}_{-43}
22	998	0.145^{+45}_{-30}
24	1072	0.101^{+31}_{-21}
26	1146	0.072^{+22}_{-15}
28	1218	0.053^{+16}_{-11}
30	1291	0.039^{+12}_{-8}
32	1364	0.030^{+9}_{-6}

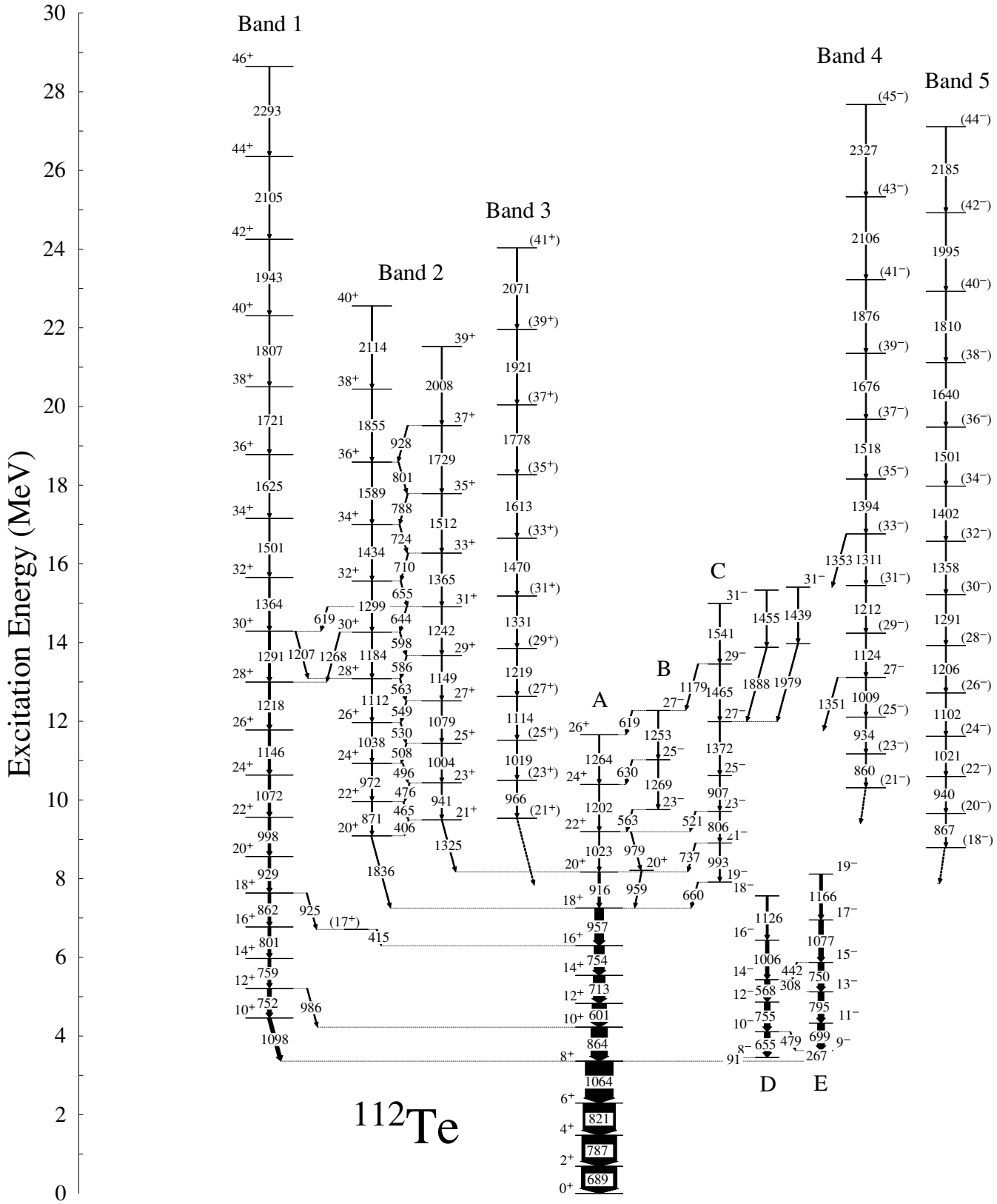

FIG. 1. The level scheme of ^{112}Te deduced from this work. Transition energies are given in keV and the widths of the arrows are proportional to the transition intensities. The tentative spin and parity assignments for Bands 3–5 are inferred through comparison with theory, whereas the absolute excitation energies of these bands are unknown.

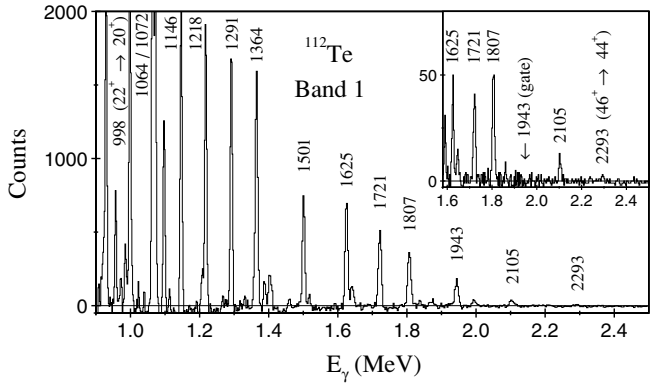

FIG. 2. Double-gated triple coincidence spectra showing transitions in Band 1 of ^{112}Te, labeled in keV, between 20^+ and 46^+. In the main spectrum, the two gates consisted of a list of all the transitions in the band, whereas in the inset, the two gates were the 1943 keV ($42^+ \rightarrow 40^+$) transition and a list of all the transitions in the band. The topmost 2293-keV transition is more evident in the inset.

$(\varepsilon_2, \varepsilon_4, \gamma)$ are [2]

$$Q_t = Q_{20}\frac{\cos(\gamma + 30^\circ)}{\cos(30^\circ)};$$
$$Q_{20} = \frac{4}{5}Zer_0^2A^{2/3}\left[\varepsilon_2\left(1+\frac{1}{2}\varepsilon_2\right)+\frac{25}{33}\varepsilon_4^2-\varepsilon_2\varepsilon_4\right]. \quad (3)$$

A possible bias of γ-ray DSAM results, caused by detecting charged particles in 4π detectors such as the Microball, has been discussed in Ref. [14]. However, in the present case this

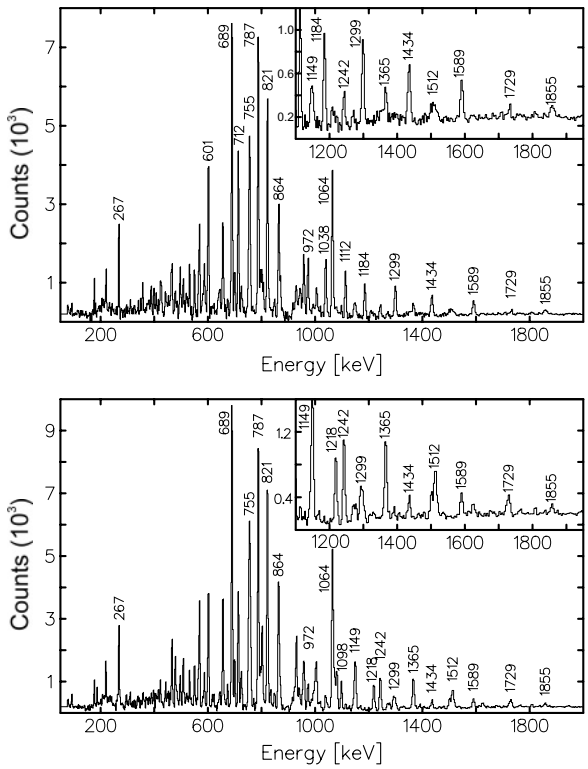

FIG. 3. Double-gated triple coincidence spectra showing the interlinked signature components of Band 2 in ^{112}Te.

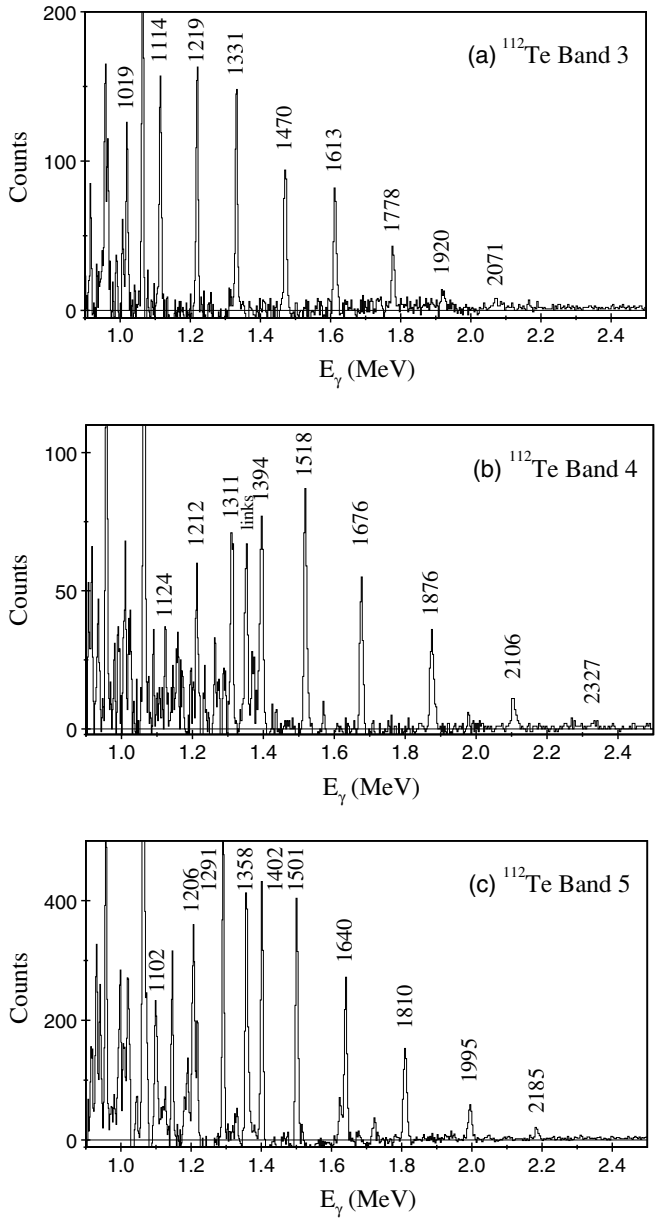

FIG. 4. Double-gated triple coincidence spectra showing transitions in Bands 3, 4, and 5, labeled in keV. In all cases, both gates consisted of a list of all the transitions in the respective bands. The peak labeled links in (b) comprises the 1353- and 1351-keV transitions depopulating Band 4, as shown in Fig. 1.

bias should not impact on the results because the residual nucleus is heavy and the number of evaporated protons large. DSAM measurements of nuclear-level lifetimes within a band can also be perturbed by the amount of sidefeeding into each level, especially if the sidefeeding is associated with structures with a quadrupole moment, Q_{sf}, that differs significantly from the in-band value Q_t. This perturbation is especially apparent when gating below a structure of interest. However, for strongly populated structures, gates can be placed *above* the levels of interest, thus eliminating any sidefeeding component. In the present analysis, it has been possible to gate on the 1291- and 1364-keV transitions above spin 28^+ and

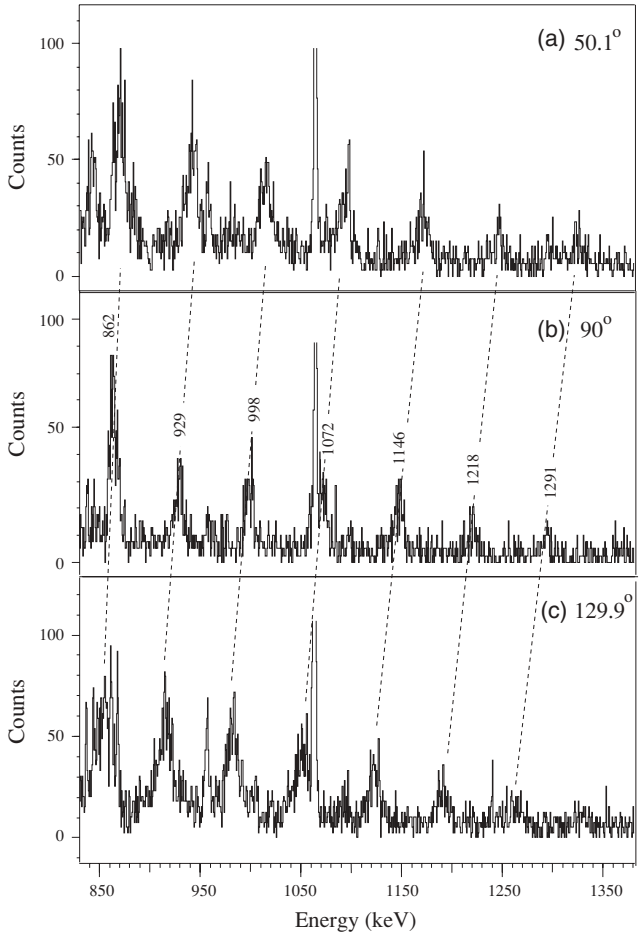

FIG. 5. Spectra produced from the sum of single gates on γ rays (1098, 752, 759 and 801 keV) in coincidence with members of Band 1 in ^{112}Te. (a) Spectrum of γ rays detected at forward angles, (b) γ rays detected at 90°, exhibiting no Doppler shift, (c) γ rays detected at backward angles.

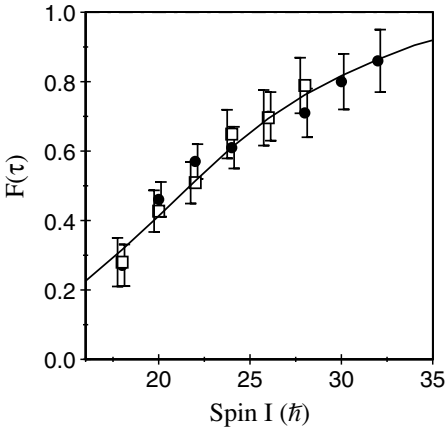

FIG. 7. Comparison of extracted $F(\tau)$ values from spectra formed by gating on transitions above spin 28$\hbar$ (gated high: open squares) and below spin 16$\hbar$ (gated low: closed circles) in Band 1 of ^{112}Te. The error bars for the gated high spectra are displayed on the left of the data points, whereas the error bars for the gated below are displayed on the right of the data points. The solid line is $F(\tau)$ calculated for $Q_t = 4.0\,eb$.

therefore remove the sidefeeding for the transitions at lower spin. Figure 7 shows the $F(\tau)$ values obtained by gating above and below the transitions of interest in Band 1. No significant difference is observed, implying that $Q_{\rm sf}$ and Q_t are very similar in magnitude.

C. Comparison to results for the ^{114}Xe isotone and ^{110}Te isotope

In the present experiment, ^{114}Xe [15,16] was populated through the ^{58}Ni(^{58}Ni, $2p\gamma$) reaction. The Microball was used to select γ rays in coincidence with two-proton evaporation and a DSAM analysis was possible for the yrast band of ^{114}Xe in the spin range 16–24$\hbar$; experimental and theoretical $F(\tau)$ values are shown in Fig. 8.

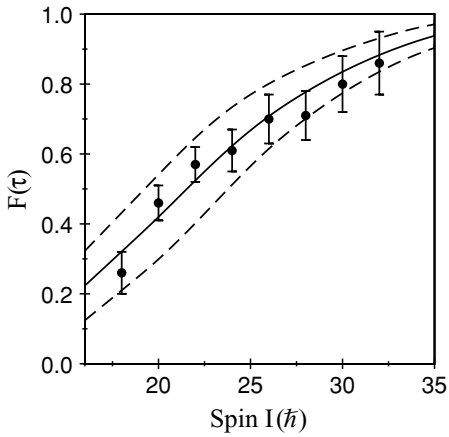

FIG. 6. $F(\tau)$ values extracted from spectra formed by gating on transitions below spin 16$\hbar$ in Band 1 of ^{112}Te. The dashed lines above and below the experimental values are calculated for $Q_t = 4.5$ and $Q_t = 3.5\,eb$, respectively. The solid line is calculated for $Q_t = 4.0\,eb$.

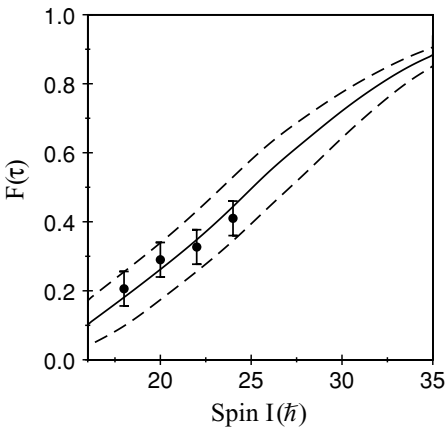

FIG. 8. $F(\tau)$ curves for the yrast band of ^{114}Xe, extracted from spectra formed by gating on transitions below spin 16$\hbar$. The dashed lines above and below the experimental values are calculated for $Q_t = 3.5$ and $Q_t = 2.5\,eb$, respectively. The solid line is calculated for $Q_t = 3.0\,eb$.

TABLE IV. Level lifetimes extracted for the yrast band of ^{114}Xe, assuming a constant $Q_t = 3.0 \pm 0.5\,eb$.

Spin I	$E_\gamma\,[I \rightarrow I-2]$ (keV)	τ (ps)
16	820	0.70^{+31}_{-19}
18	879	0.49^{+21}_{-10}
20	937	0.35^{+15}_{-9}
22	997	0.26^{+11}_{-7}
24	1062	0.19^{+8}_{-5}

A value of $Q_t = 3.0 \pm 0.5\,eb$ was extracted for this band, which translates to a quadrupole deformation of $\varepsilon_2 = 0.19 \pm 0.03$, assuming zero hexadecapole deformation and axial, prolate nuclear shape. Extracted mean level lifetimes, corresponding to $Q_t = 3.0 \pm 0.5\,eb$, are listed in Table IV.

Although it was not possible to measure the lifetimes of levels in Band 3 of ^{112}Te, it was possible to extract lifetimes of an analogous strongly coupled band in ^{110}Te, as reported in Ref. [11]. In this case, the Microball was used to select the $\alpha 2p$ evaporation channel leading to ^{110}Te. Lifetimes were extracted through a Doppler broadened line-shape (DBLS) analysis [9] of $\Delta I = 1$ transitions in the spin range 21–23$\hbar$. An average value of $Q_t = 2.8\,eb$ was extracted that translates into a quadrupole deformation of $\varepsilon_2 \approx 0.18$, assuming zero hexadecapole deformation and axial, prolate nuclear shape. From the present data, it was not, however, possible to measure lifetimes of any of the $\Delta I = 2$ intruder bands in ^{110}Te [17,18].

IV. DISCUSSION

To assign configurations to the bands in ^{112}Te, calculations have been performed using the configuration-dependent cranked Nilsson-Strutinsky (CNS) approach [2,19,20]. Calculated configurations are labeled using the $[p_1 p_2, n]$ nomenclature of Ref. [19], where p_1 represents the number of $\pi g_{9/2}$ holes, p_2 represents the number of $\pi h_{11/2}$ particles, and n represents the number of $\nu h_{11/2}$ particles, relative to the $Z = N = 50$ doubly magic core. Pairing correlations are neglected in the CNS formalism.

In the following discussion, experiment and theory are presented in "rigid-rotor" plots, where energies are plotted relative to a rotating liquid-drop reference, $E_{\rm RLD} \propto I(I+1)$. In such diagrams, energies of smooth terminating bands tend to decrease to a minimum value before increasing again for states approaching the limiting angular momentum at termination. The slopes of such plots, together with the position of the minimum in the $(E - E_{\rm RLD})$ energy, are highly sensitive to the spin values assigned to a band and thus may be used to assign (tentative) spin values through comparison of experiment with theory. Such is the case for the unlinked Bands 3–5; Fig. 1 shows these tentative assignments. With these assignments, experimental counterparts are found for those configurations that are calculated to be lowest in energy for spin values $\approx$30–50$\hbar$. Indeed, a somewhat more complete plot of the calculated bands was previously published in Fig. 26 of Ref. [2].

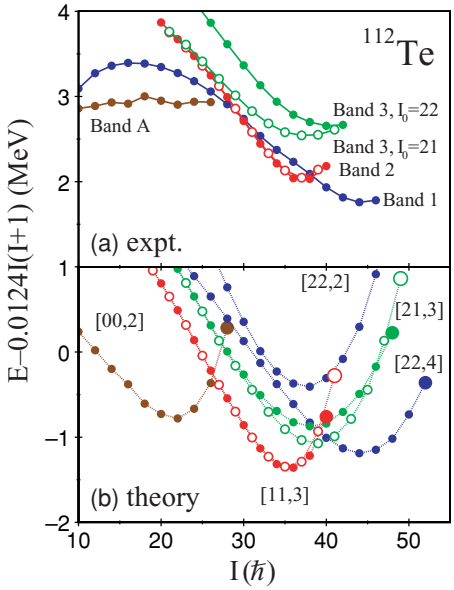

FIG. 9. (Color online) Experimental and theoretical rigid-rotor plots for ^{112}Te. Only positive-parity states are shown with solid circles corresponding to states with signature $\alpha = 0$ and open circles to $\alpha = 1$. In (b) large symbols indicate terminating states with $\gamma = 60°$. Experimental data for Band 3 are included in (a) based on the given band-head assignments of $I_0 = 21$ and 22. Note that the absolute excitation energy of Band 3 is not known.

Table V summarizes the adopted band assignments through comparison with the CNS calculations. Predicted low-spin (prolate) and high-spin (oblate) deformations are also listed. The configuration assignments are discussed in the following Sections.

TABLE V. CNS $[p_1 p_2, n]$ band assignments and average predicted quadrupole deformations at low spin (prolate: $\gamma \sim 0°$) and at termination (oblate: $\gamma = 60°$).

	Configuration	Signature α	ε_2 (low spin)	Terminating spin	ε_2 (at termination)
Band 1	[22,4]	0	0.28	52^+	0.15
Band 2	[11,3]	0	0.22	40^+	0.17
Band 2	[11,3]	1	0.22	41^+	0.15
Band 3	[21,3]	1	0.25	49^+	0.12
Band 4	[22,3]	1	0.26	49^-	0.16
Band 5	[22,3]	0	0.26	50^-	0.15

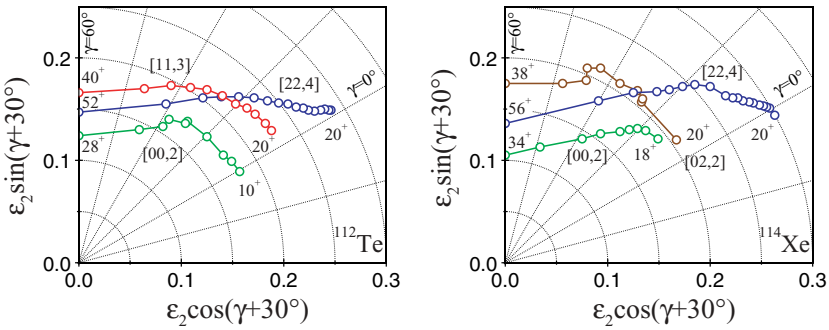

FIG. 10. (Color online) Calculated shape trajectories as a function of spin for bands built upon specific positive-parity configurations in ^{112}Te and ^{114}Xe. They are shown in steps of $2\hbar$ with initial and final spins indicated.

A. Positive-parity configurations

Experimental and theoretical energies, relative to a rotating liquid-drop reference, are shown in Fig. 9 for positive-parity states and configurations in ^{112}Te. Band 1 is well described by the [22,4] configuration at high spin. Moreover, an energy minimum occurs at $44\hbar$ in both theory and experiment. Band 1 is seen up to $I^{\pi} = 46^{+}$, just 6 units of spin below the terminating spin of $I^{\pi} = 52^{+}$ for the theoretical [22,4] configuration. The strongly coupled Band 2 is assigned to the [11,3] configuration; this configuration, with a single $\pi g_{9/2}$ hole in the [404]$9/2^{+}$ Nilsson orbital, yields degenerate signature $E2$ partners, while enhancing the $M1$ strength of interlinking dipole transitions. This is evident in Fig. 1, where the dipole transitions in Band 2 are seen to energies in excess of 900 keV. Smooth terminating dipole bands based an a single $\pi g_{9/2}$ hole are extremely rare in this mass region. Indeed, apart from Band 2 in ^{112}Te, the only other examples of these structures have been found in ^{110}Te, from the present data, where two such terminating dipole structures have been observed [11]. One signature of the strongly coupled Band 2 in ^{112}Te achieves termination at $I^{\pi} = 40^{+}$, whereas the other signature, reaching $I^{\pi} = 39^{+}$, is just one transition away from termination.

Unlinked Band 3 is also included in Fig. 9(a), with assumed band-head spins of 21 and 22, and is assigned to the [21,3] configuration of Fig. 9(b). Note that both signature $\alpha = 0$ and $\alpha = 1$ components of the calculated [21,3] configuration are drawn with the odd-spin $\alpha = 1$ component lowest in energy at high spin, $\sim 40\hbar$. The general shape of the curve generated for Band 3 with a band-head spin of 21 matches well the $\alpha = 1$ component of the [21,3] configuration. Hence a band-head assignment of $I^{\pi} = (21^{+})$ is adopted in Fig. 1.

Smooth terminating bands built on the [22,4] configuration have also been observed down to low spin, $\sim 10\hbar$, in the ^{114}Te [21] and ^{116}Te [22] isotopes. In addition, a smooth terminating band associated with the [22,4] configuration has been observed in the ^{114}Xe isotone in the spin range 26–$52\hbar$ [16]; it is predicted to terminate at $I^{\pi} = 56^{+}$ in this nucleus. Theoretical shape trajectories through the ε_2-γ plane are shown in Fig. 10 for positive-parity configurations in ^{112}Te and ^{114}Xe. In each nucleus, the [22,4] configuration is predicted to be well-deformed prolate ($\varepsilon_2 \sim 0.28 - 0.30$) at low spin ($\sim 20\hbar$) but the quadrupole deformation is significantly less ($\varepsilon_2 \sim 0.14$) at termination into an oblate ($\gamma = 60^{\circ}$) shape. In the case of ^{114}Xe, the extracted Q_t value for the yrast band indicates that the deformed [22,4] configuration has not yet been reached by spin $24\hbar$. Indeed, the measurements are more consistent with the theoretical [02,2] or [00,2] configurations in this spin range, which contain no $\pi g_{9/2}$ holes.

Theoretical transition quadrupole moments are shown in Fig. 11 for ^{112}Te. These were obtained from the CNS deformations using Eq. (3). The experimental result for Band 1 in ^{112}Te, of $Q_t = 4.0 \pm 0.5\, eb$ in the spin range 18–$32\hbar$, is also indicated on the figure. The experimental result lies between the [22,2] and [22,4] configurations and may indicate a degree of mixing between these pure configurations in this spin range. Indeed, it can be seen in Fig. 9(b) that these two configurations become close in energy for spin below $30\hbar$. Note that the average calculated value of γ in the spin range 18–$32\hbar$ is approximately 6°, which means that $Q_t = 4.0 \pm 0.5\, eb$ translates to a slightly larger ε_2 deformation than quoted in Sec. III B, namely $\varepsilon_2 = 0.27 \pm 0.03$.

B. Deformation systematics

The deformation-driving $\pi g_{9/2}^{-2} h_{11/2}^{2}$ (2p-2h) excitation is believed to be a crucial ingredient of the superdeformed bands in ^{132}Ce [23]. Furthermore, structures involving two proton $g_{9/2}$ holes, with an enhanced deformation relative to the ground states [24], can be followed all the way from the smooth terminating bands in the mass 110 region up to the superdeformed bands in the mass 150 region around ^{152}Dy. Experimental quadrupole deformations, extracted from measured quadrupole moments, are shown in Fig. 12, together with average theoretical CNS values. A clear systematic

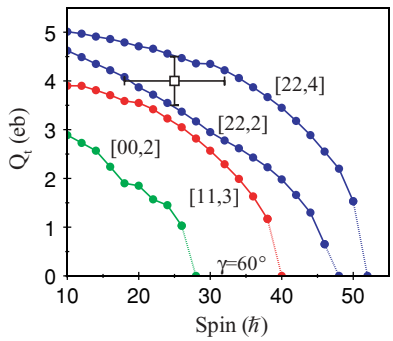

FIG. 11. (Color online) Theoretical and experimental quadrupole moments for ^{112}Te. The average experimental value for Band 2 is shown by the open square. Theoretical Q_t values drop to zero at termination into noncollective oblate shapes with $\gamma = 60^{\circ}$.

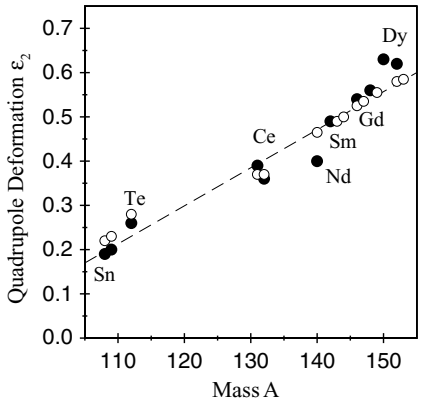

FIG. 12. Average experimental quadrupole deformations, ε_2, extracted from measured quadrupole moments of $\pi g_{9/2}^{-2}$ bands over a wide mass range (solid circles). Theoretical CNS deformations are also included (open circles). In extracting these values, it was assumed $\varepsilon_4 = 0$ and $\gamma = 0^\circ$. The structures range from a smooth terminating band in ^{108}Sn right up to the (yrast) superdeformed band in ^{152}Dy. The dashed line is drawn to guide the eye.

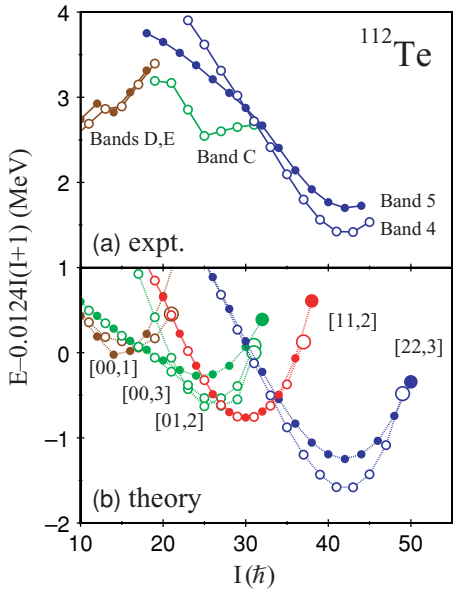

FIG. 13. (Color online) Experimental and theoretical rigid-rotor plots for negative-parity configurations in ^{112}Te. Solid circles in (b) correspond to states with signature $\alpha = 0$ and open circles to $\alpha = 1$. Large symbols indicate terminating states with $\gamma = 60^\circ$. Experimental data for Bands 4 and 5 are shown in (a) based on the spin assignments shown in Fig. 1; these values are only tentative. Note that the absolute excitation energies of Bands 4 and 5 are not known.

behavior is observed of increasing deformation with particle number as discussed in Ref. [25]. This pattern is formed along the $g_{9/2}$ proton orbital but can also be seen as a manifestation of the typical valleys and ridges seen in the shell-energy landscape when it is considered as a function of particle number and quadrupole deformation. Equatorial upsloping orbitals are degenerate in the harmonic oscillator and, excluding the high-j intruder orbitals, close to degenerate in realistic nuclear potentials; referred to as a pseudo-SU(3) (or pseudo-oscillator) symmetry in Ref. [26]. These close to degenerate orbitals give rise to a high level density and consequently ridges of high unfavored shell energy. It is then the valleys of favored shell energy formed in between these ridges that explain the systematic features seen in Fig. 12.

C. Negative-parity configurations

Experimental and theoretical energies, relative to a rotating liquid-drop reference, are shown in Fig. 13 for negative-parity configurations in ^{112}Te. Theory shows a succession of configurations terminating progressively at spin $\sim 20\hbar$, $\sim 30\hbar$, $\sim 36\hbar$, and finally $\sim 50\hbar$. Band C of Fig. 1 is followed up to $I^\pi = 31^-$, which is the terminating state of both [00,3] and [01,2] configurations in Fig. 13(b). Hence it probably corresponds to one of (or a mixture of) these configurations.

A strongly coupled negative-parity configuration, namely the [11,2] configuration, extends to spin $\sim 36\hbar$ in Fig. 13(b). This structure is analogous to the [11,3] positive-parity configuration assigned to Band 2; however, no experimental evidence could be found for a second strongly coupled band in ^{112}Te, although two such bands have been established in ^{110}Te [11].

It can be seen in Fig. 13(b) that theoretical signature-partner [22,3] configurations dominate at high spin above $35\hbar$. Because Bands 4 and 5 decay to negative-parity states in ^{112}Te, and are both seen to high γ-ray energy (and hence spin), it seems plausible to associate these bands with the [22,3] configuration. Because Band 4 feeds odd-spin, negative-parity states, i.e., Band C, signature $\alpha = 1$ is chosen for this band. It follows that Band 5 then has even spin and signature $\alpha = 0$. This assumption now limits the assigned spins of the bands to units of $2\hbar$. The values shown in Fig. 1 produce the experimental rigid-rotor plots of Fig. 13(a) that match very well the theoretical [22,3] curves, in particular the slopes and position of energy minima at 42^- and 43^-. Note, however, that neither the absolute excitation energy nor the relative excitation energy of Bands 4 and 5 are known. Above spin $35\hbar$, the slope of the $\alpha = 1$ component of the [22,3] configuration is steeper than that of the $\alpha = 0$ component, which is also observed experimentally. Below this spin value, the slope of Band 5 becomes less steep and may reflect a mixing of the pure $\alpha = 0$ [22,3] and [00,3] theoretical configurations.

V. CONCLUSIONS

High-spin experiments have been performed to study the level structure of ^{112}Te and several smooth terminating bands have been established, one of which is a strongly coupled structure. Cranked Nilsson-Strutinsky calculations have been used to assign configurations to the bands. In addition, lifetime measurements have been performed for the strongest band and clearly show a large quadrupole deformation for this structure. The calculations indicate that this deformed structure is built

on a $\pi g_{9/2}^{-2} h_{11/2}^{2}$ configuration, relative to the $Z = 50$ shell closure.

Apart from the present work, lifetime measurements of smooth terminating bands in the mass 110 region have only been reported for ^{108}Sn and ^{109}Sb [3]. However, taken with the results for ^{112}Te, a systematic behavior of quadrupole deformation emerges bridging the mass 110, mass 130, and mass 150 regions of the nuclear landscape.

ACKNOWLEDGMENTS

This work was supported in part by the DOE grants DE-F05-96ER-40983, DE-FG02-07ER41459, the U.S. National Science Foundation, the UK Engineering and Physical Sciences Research Council, the U.S. National Research Council under the Collaboration in Basic Science and Engineering Program, and by the Swedish Science Research Council.

[1] I. Ragnarsson, V. P. Janzen, D. B. Fossan, N. C. Schmeing, and R. Wadsworth, Phys. Rev. Lett. **74**, 3935 (1995).
[2] A. V. Afanasjev, D. B. Fossan, G. J. Lane, and I. Ragnarsson, Phys. Rep. **322**, 1 (1999).
[3] R. Wadsworth *et al.*, Phys. Rev. Lett. **80**, 1174 (1998).
[4] I. Y. Lee, Nucl. Phys. **A520**, 641c (1990).
[5] D. G. Sarantites, P. -F. Hua, M. Devlin, L. G. Sobotka, J. Elson, J. T. Hood, D. R. LaFosse, J. E. Sarantites, and M. R. Maier, Nucl. Instrum. Methods A **381**, 418 (1996).
[6] D. C. Radford, Nucl. Instrum. Methods A **361**, 297 (1995).
[7] D. C. Radford, Nucl. Instrum. Methods A **361**, 306 (1995).
[8] D. Seweryniak, J. Nyberg, C. Fahlander, and A. Johnson, Nucl. Instrum. Methods A **340**, 353 (1994).
[9] P. J. Nolan and J. F. Sharpey-Schafer, Rep. Prog. Phys. **42**, 1 (1979).
[10] E. S. Paul *et al.*, Phys. Rev. C **50**, 698 (1994).
[11] A. O. Evans *et al.*, Phys. Lett. **B636**, 25 (2006).
[12] R. M. Clark *et al.*, Phys. Rev. Lett. **76**, 3510 (1996).
[13] J. F. Ziegler, *The Stopping and Ranges of Ions in Matter* (Pergamon, London, 1985), Vols. 3 and 5.
[14] C. J. Chiara, D. R. LaFosse, D. G. Sarantites, M. Devlin, F. Lerma, and W. Reviol, Nucl. Instrum. Methods A **523**, 374 (2004).
[15] E. S. Paul *et al.*, Nucl. Phys. **A673**, 31 (2000).
[16] E. S. Paul *et al.*, Phys. Rev. C **65**, 051308(R) (2002).
[17] A. J. Boston, Ph. D. thesis, University of Liverpool (2000).
[18] E. S. Paul *et al.*, Phys. Rev. C submitted, CX10034 (2006).
[19] A. V. Afanasjev and I. Ragnarsson, Nucl. Phys. **A591**, 387 (1995).
[20] T. Bengtsson and I. Ragnarsson, Nucl. Phys. **A436**, 14 (1985).
[21] I. Thorslund, D. B. Fossan, D. R. LaFosse, H. Schnare, K. Hauschild, I. M. Hibbert, S. M. Mullins, E. S. Paul, I. Ragnarsson, J. M. Sears, P. Vaska, and R. Wadsworth, Phys. Rev. C **52**, R2839 (1995).
[22] J. M. Sears, D. B. Fossan, I. Thorslund, P. Vaska, E. S. Paul, K. Hauschild, I. M. Hibbert, R. Wadsworth, S. M. Mullins, A. V. Afanasjev, and I. Ragnarsson, Phys. Rev. C **55**, 2290 (1997).
[23] A. V. Afanasjev and I. Ragnarsson, Nucl. Phys. **A608**, 176 (1996).
[24] I. Ragnarsson, Acta Phys. Pol. B **27**, 33 (1996).
[25] I. Ragnarsson, S. G. Nilsson, and R. K. Sheline, Phys. Rep. **45**, 1 (1978).
[26] J. Dudek, W. Nazarewicz, Z. Szymanski, and G. A. Leander, Phys. Rev. Lett. **59**, 1405 (1987).